Materials Advances

ROYAL SOCIETY OF CHEMISTRY

PAPER

View Article Online
View Journal | View Issue

Cite this: *Mater. Adv.*, 2024, 5, 5579

2,2′-Bipyridine-4,4′-dicarboxylic acid ligand engineered $CsPbBr_3$ perovskite nanocrystals for enhanced photoluminescence quantum yield with stable display applications†

Ankit Kumar,[a] Sukanya Ghosh,[a] Ankush Saini,[b] Sumit Kumar,[a] Monojit Bag *[b] and Prasenjit Kar *[a]

Received 8th February 2024,
Accepted 20th May 2024

DOI: 10.1039/d4ma00124a

rsc.li/materials-advances

Cesium lead halide perovskite nanocrystals (PNCs) have emerged over the last decade as a promising candidate for optoelectronic devices, owing to their exceptional optical and color-tunable properties. Despite this, the instability of these materials and reduction in the photoluminescence (PL) properties with time prevents them from reaching their potential applications in the real world. The degradation in the PL properties of PNCs is due to surface defects caused by the removal of surface ligands. Herein, we have used a bidentate ligand, namely 2,2′-bipyridine-4,4′-dicarboxylic acid (BPY), to improve the optical properties of green-emitting $CsPbBr_3$ PNCs such as PL, and photoluminescence quantum yield (PLQY). The surface defects are reduced by the coordination of the carboxyl group of the bidentate BPY ligand with under-coordinated lead atoms. The PLQY of pristine $CsPbBr_3$ PNCs increased from 64 ± 2% to 88 ± 2% for BPY-$CsPbBr_3$ PNCs. In addition, a down-converted green light-emitting diode (LED) was fabricated by utilizing BPY-$CsPbBr_3$ PNCs, which shows its potential in display applications. Thus, our results will promote these inorganic PNCs in the commercial development of optoelectronic devices.

Introduction

Recently, lead halide perovskites (LHPs) have grabbed significant attention from the scientific community.[1,2] The scrutiny towards LHPs is due to their exceptional optical and electrical properties, such as high PLQY,[3,4] broad absorption over the whole visible region, intense PL with a very narrow width of the emission,[5] tunable band gap,[6] high charge-carrier diffusion,[7] and high tolerance factor,[8] *etc.* With all these superior properties, LHPs have been extensively used in optoelectronic devices, such as light emitting diodes (LEDs),[9] solar cells,[10] photodetectors,[11] lasers,[12] and wide color gamut displays.[13] Additionally, the low fabrication cost and easy synthetic approach make these materials more suitable for use in the field of optoelectronic devices. However, with all these exceptional achievements, LHPs are not able to achieve practical applications because of their toxicity and instability towards heat, moisture, and light.[14]

There are numerous methods to enhance the stability of LHPs, such as encapsulation with other semiconductor material shells, encapsulation with mesoporous materials like metal–organic frameworks and covalent organic frameworks, and surface passivation with different types of ligands.[15–19] Recently, it was found that surface passivation with capping ligands is an efficient way to enhance the stability and optical properties of LHPs.[20,21] The bonding between the surface of nanocrystals and the capping ligands is highly dynamic in nature; due to this, perovskite materials suffer from intrinsic chemical instability.[22] The ligands detach from the surface of perovskite nanocrystals with aging, washing, and dilution. All these processes lead to the generation of defects on the surface of nanocrystals.[23] These surface defects are responsible for nonradiative recombination. The combination of these defects leads to a decrease in the optical properties, stability, and performance of the device. Therefore, it is critical to understand the role of surface defects in limiting device performance and developing new routes to passivate the surface defects to increase device performance.

Oleic acid (OA) and oleylamine (OAm) are one of the most familiar acid–base pairs of capping ligands that have been

[a] *Department of Chemistry, Indian Institute of Technology Roorkee, Roorkee, Uttarakhand, India. E-mail: kar.prasen@gmail.com, prasenjit.kar@cy.iitr.ac.in*
[b] *Department of Physics, Indian Institute of Technology Roorkee, Roorkee, Uttarakhand, India. E-mail: monojit.bag@ph.iitr.ac.in*

† Electronic supplementary information (ESI) available: FTIR spectra and ^{1}H NMR spectrum of BPY, SEM images, elemental mapping, EDX spectra of pristine $CsPbBr_3$ PNCs and BPY-$CsPbBr_3$ PNCs, and FTIR and PLQY spectra of BPY-$CsPbBr_3$ PNCs. XPS survey scan of pristine $CsPbBr_3$ PNCs and BPY-$CsPbBr_3$ PNCs, and photographs of the down-converted LED under daylight. See DOI: https://doi.org/10.1039/d4ma00124a

regularly used by a number of research groups in the synthesis of perovskite nanomaterials.[24,25] OA capped the surface of the LHPs by the coordination of its carboxyl group with Pb, while OAm capped the surface through hydrogen bonding with halogen (X) by its protonated ammonium group. However, this pair of ligands acts as an insulating layer on the surface of nanocrystals, which hampers the charge carriers and reduces the performance of the device.[26] Nowadays, along with OA and OAm, different capping ligands are used during different passivation techniques, such as post-synthesis and *in situ* synthesis.[27–29] Alivisatos *et al.* demonstrate that post-treatment of $CsPbBr_3$ nanocrystals with thiocyanate salt increases the PLQY as well as the stability of the synthesized nanocrystal.[30] The combination of trioctylphosphine with PbI_2 (TOP-PbI_2) is used as a precursor for the synthesis of phase-stable $CsPbBr_3$ nanocrystals with unity PLQY.[31] Pan *et al.* have synthesized $CsPbI_3$ nanocrystals with improved stability and near-unity PLQY with post-synthesis passivation by the use of a bidentate ligand 2,2′-iminodibenzoic acid.[26] Zhu *et al.* have improved the PLQY near unity *via* the post-synthetic modification with $ZnBr_2$.[32] Pradhan *et al.* brought the PLQY of all LHPs closer to unity by developing a simple synthetic method based on the use of alkylammonium halide salt, which serves both as a source of halides and as a capping ligand at the same time.[33]

Here, we have reported the synthesis of BPY-$CsPbBr_3$ PNCs using OAm and a bidentate ligand (BPY) in place of conventionally used OA as a capping ligand (Scheme 1). Bidentate ligands strongly bind with the Pb^{2+} atom as compared to the monodentate ligands.[26,34] As a result, the stability of the nanocrystals increased, which further improved the optical properties of the perovskite nanocrystals. The effect of the BPY ligand on the optical properties was studied by performing optical studies. The BPY ligand enhances the optical properties and the BPY-$CsPbBr_3$ PNCs show PLQY (88 ± 2%) that is much higher than that of pristine $CsPbBr_3$ PNCs (64 ± 2%). Furthermore, the stability of BPY-$CsPbBr_3$ PNCs in the ambient environment and against heat was investigated. Finally, a down-converted green LED was fabricated using BPY-$CsPbBr_3$ PNCs.

Experimental details

Materials

Lead bromide ($PbBr_2$, 99.99%), oleylamine (OAm, technical grade, 70%), and octadecene (ODE, technical grade, 70%) were procured from Sigma-Aldrich. Hexane and hydrochloric acid (HCl) were purchased from Rankem. Oleic acid (OA, 90%, Alfa Aesar), sodium dichromate ($Na_2Cr_2O_7{\cdot}2H_2O$, Himedia), sulfuric acid (H_2SO_4, Finar), 4,4′-dimethyl-2,2′-bipyridine (Loba Chemicals), sodium hydroxide (NaOH, SRL), and cesium carbonate (Cs_2CO_3, Avra chemicals, 98%) were ordered from local vendors. All the chemicals were utilized without being further purified.

Synthesis of 2,2′-bipyridine-4,4′-dicarboxylic acid (BPY)

0.50 g (2.71 mmol) of 4,4′dimethyl-2,2′-bipyridine was gradually added to a solution of 1.81 g (6.09 mmol) of $Na_2Cr_2O_7{\cdot}2H_2O$ in 7 mL of concentrated sulfuric acid under constant magnetic stirring. The resulting mixture became orange, and after a few minutes, the color changed to green, and the reaction was accomplished after 30 minutes. After that, the reaction mixture was poured into 100 mL of cold water, resulting in a light-yellow precipitate. Following filtration and drying, the solid was dissolved in an alkaline 10% NaOH aqueous solution, which was then slowly acidified using a 10% aqueous HCl solution. This recrystallization produced the desired product, which was free from Cr (+3) ions. After filtration and drying in a vacuum, the final white solid was collected.

Preparation of cesium oleate

Cs_2CO_3 (0.407 g) was loaded into a 50 ml two-neck flask along with ODE (15 ml), and then degassed at 120 °C for 20 minutes. After that, 1.5 ml OA was injected, and the reaction mixture was heated under an N_2 atmosphere at 120 °C for 2 h. Cs-oleate was preheated at 80 °C before injection because it is precipitated out from ODE at room temperature.

Synthesis of BPY-$CsPbBr_3$ PNCs

ODE (5 ml), $PbBr_2$ (0.0367 g, 0.1 mmol), and BPY (20 mg) were degassed for 1 hour at 120 °C in a 50 ml three-neck flask. OAm (0.5 ml) was injected under N_2 at 120 °C. After the complete dissolution of $PbBr_2$, the temperature of the reaction was increased to the required temperature of 160 °C. Under N_2, preheated (80 °C) Cs-oleate (0.4 ml) was injected, and the reaction mixture was heated for 20 s. The reaction mixture was cooled to room temperature in an ice bath. The supernatant was removed after centrifuging the crude solution at 6000 rpm for 10 minutes, and the remaining solid precipitate was redispersed in hexane. After repeating this procedure,

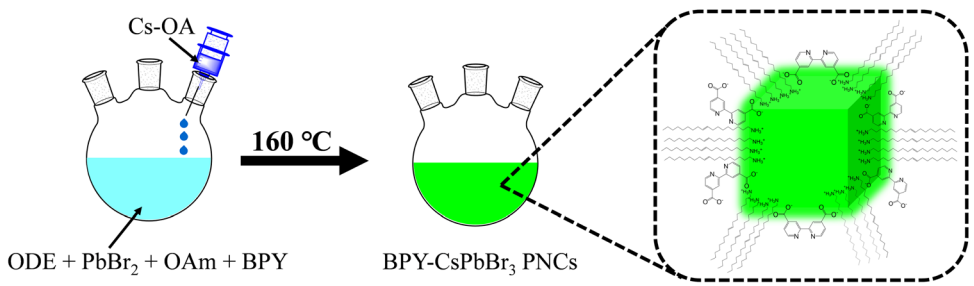

Scheme 1 Synthesis of BPY-$CsPbBr_3$ PNCs.

the solid precipitate was redispersed in hexane for further characterization.

Synthesis of pristine $CsPbBr_3$ PNCs

ODE (5 ml) and $PbBr_2$ (0.0367 g, 0.1 mmol) were degassed for 1 hour at 120 °C in a 50 ml three-neck flask. OAm (0.5 ml) and OA (0.5 ml) were injected under N_2 at 120 °C. After that, all the remaining steps are the same as above.

LED device fabrication

A down-converted green LED was fabricated by coating BPY-$CsPbBr_3$ PNCs on a commercially available blue LED (λ_{ex} = 395 nm).

Material characterization

The optical properties of the synthesized nanocrystals were recorded by performing UV-vis, PL, PLQY, and TCSPC studies. The formation of the nanocrystals was confirmed by XRD analysis. Morphology, crystallinity, and crystal size were confirmed by using TEM analysis. Furthermore, SEM studies support the TEM analysis. The presence of BPY ligand on the nanocrystal surface was confirmed by performing FTIR and XPS studies. For the stability data, time-dependent XRD and PL studies were performed. For thermal stability, the TGA technique was utilized. We also synthesized the BPY ligand and the formation of BPY was confirmed by FTIR and NMR analysis (Fig. S1 and S2, ESI†).

Results and discussion

The synthesis of $CsPbBr_3$ PNCs was carried out using the widely recognized synthetic technique of hot injection (HI).[35] Cs-oleate and $PbBr_2$ were used as precursors along with OAm, OA, and BPY as capping ligands. The as-synthesized $CsPbBr_3$ PNCs were redispersed in hexane after purification for further characterization. $CsPbBr_3$ PNCs were synthesized utilizing OA and OAm represented as pristine $CsPbBr_3$ PNCs, while $CsPbBr_3$ PNCs were synthesized utilizing BPY and OAm represented as BPY-$CsPbBr_3$ PNCs.

Fig. 1(a) depicts the XRD patterns of pristine $CsPbBr_3$ PNCs and BPY-$CsPbBr_3$ PNCs. The XRD analysis implies that the XRD patterns of both the nanocrystals are well indexed with the cubic phase.[36] All the diffraction peaks obtained in the XRD pattern at 2θ = 15.20°, 21.45°, 30.55°, 34.18°, 37.65°, and 43.67°, well resemble the corresponding planes of (100), (110), (200), (210), (211), and (220), respectively. XRD analysis confirmed that no structural changes occur between the pristine $CsPbBr_3$ PNCs and BPY-$CsPbBr_3$ PNCs. Additionally, similarities in structural properties were further supported by transmission electron microscopy (TEM) analysis. The TEM images of BPY-$CsPbBr_3$ PNCs and pristine $CsPbBr_3$ PNCs are depicted in Fig. 1(b) and (e), respectively.

The TEM images indicate that both the nanocrystals exhibit a uniform cubic morphology. The high crystallinity of the nanocrystals was confirmed by using selected area electron diffraction (SAED) (Fig. 1(c) and (f)). The average crystal size of pristine $CsPbBr_3$ PNCs and BPY-$CsPbBr_3$ PNCs is ~11.5 and ~15 nm, respectively (Fig. 1(d) and (g)). The morphology of the nanocrystals was further examined by scanning electron microscopy (SEM). The SEM images also reveal that nanocrystals acquire a cubic morphology. The SEM images of the pristine $CsPbBr_3$ PNCs and BPY-$CsPbBr_3$ PNCs are presented in Fig. S3 and S4 (ESI†), respectively. The energy-dispersive X-ray spectroscopy (EDX) analysis indicates the presence of all respective elements, as depicted in Fig. S3 and S4 (ESI†). Elemental mapping of the SEM images demonstrates the uniform distribution of all the elements throughout the surface of the nanocrystals (Fig. S3 and S4 (ESI†)). These studies prove that there are no changes between the structural properties of pristine $CsPbBr_3$ PNCs and BPY-$CsPbBr_3$ PNCs.

However, we observed a significant change in the optical properties between pristine $CsPbBr_3$ PNCs and BPY-$CsPbBr_3$ PNCs. The absorbance and PL spectra of pristine $CsPbBr_3$ PNCs

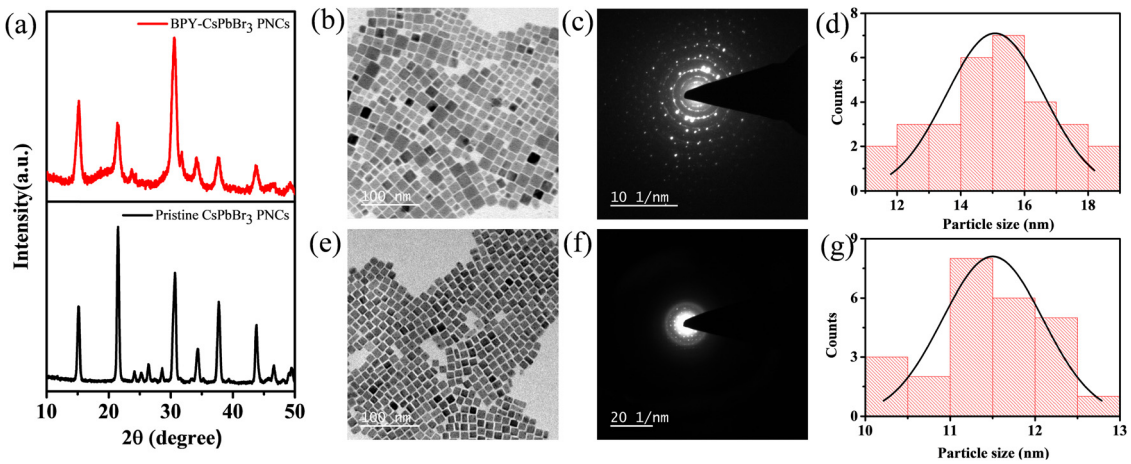

Fig. 1 (a) XRD pattern of BPY-$CsPbBr_3$ PNCs and pristine $CsPbBr_3$ PNCs; TEM images of (b) BPY-$CsPbBr_3$ PNCs, and (e) pristine $CsPbBr_3$ PNCs; SAED pattern of (c) BPY-$CsPbBr_3$ PNCs and (f) pristine $CsPbBr_3$ PNCs; particle size distribution curve of (d) BPY-$CsPbBr_3$ PNCs and (g) pristine $CsPbBr_3$ PNCs.

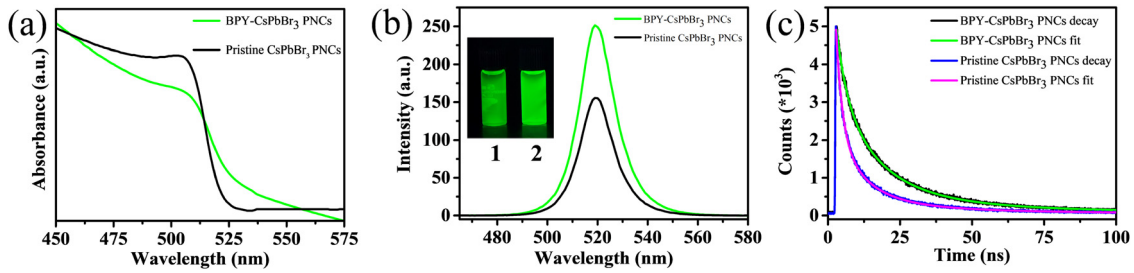

Fig. 2 (a) UV-Vis; (b) PL (inset shows the optical images of 1 pristine $CsPbBr_3$ PNCs and 2 BPY-$CsPbBr_3$ PNCs); (c) TCSPC spectra of pristine $CsPbBr_3$ PNCs and BPY-$CsPbBr_3$ PNCs.

and BPY-$CsPbBr_3$ PNCs are presented in Fig. 2(a) and (b), respectively. The characteristic absorption and emission peaks of $CsPbBr_3$ PNCs are exhibited at 504 and 519 nm, respectively. There is an improvement in the PL and PLQY for BPY-$CsPbBr_3$ PNCs. The PLQY improved from 64 ± 2% for pristine $CsPbBr_3$ PNCs to 88 ± 2% for BPY-$CsPbBr_3$ PNCs (Fig. S5, ESI†). To understand the origin of the PL enhancement of BPY-$CsPbBr_3$ PNCs, time-correlated single-photon counting (TCSPC) analysis was used. Fig. 2(c) shows the TCSPC curves of both the nanocrystals in hexane using a 450 nm LED as an excitation source. All the TCSPC curves are well-fitted with an exponential function (eqn (1)).

$$\text{Fit} = B + A_1\exp(-t/\tau_1) + A_2\exp(-t/\tau_2) + A_3\exp(-t/\tau_3) \quad (1)$$

$$\tau_{avg} = \frac{A_1\tau_1^2 + A_2\tau_2^2 + A_3\tau_3^2}{A_1\tau_1 + A_2\tau_2 + A_3\tau_3} \quad (2)$$

$$\text{PLQY} = \frac{k_r}{k_r + k_{nr}} = \tau_{avg}k_r \quad (3)$$

Here, τ_1, τ_2, and τ_3 are lifetime components. A_1, A_2, and A_3 are the coefficients of the weight fraction corresponding to the τ_1, τ_2, and τ_3 lifetime components, respectively. τ_1 is the shortest decay component that corresponds to a trap state or nonradiative recombination. τ_2 is the middle decay component that corresponds to band edge recombination. τ_3 is the longest decay component attributed to shallow trap-mediated recombination.[37–39] The average lifetime (τ_{avg}) was calculated by using eqn (2). The nonradiative recombination rate (K_{nr}) and radiative recombination rate (K_r) were calculated using eqn (3). Table 1 summarizes the τ_1, τ_2, τ_3, A_1, A_2, A_3, PLQY, and calculated τ_{avg}, K_{nr}, and K_r. The τ_{avg} increases from 20.67 ns for pristine $CsPbBr_3$ PNCs to 25.80 ns for BPY-$CsPbBr_3$ PNCs, which is similar to the PLQY results. Furthermore, the K_r increases and K_{nr} decreases, which is consistent with the coefficients of recombination. The contribution of A_1 decreases, which is responsible for nonradiative recombination, while the contribution of A_2 and A_3 increases. Therefore, we can conclude that the BPY capping ligand effectively passivates the surface defects and reduces the nonradiative recombination, thus improving the PL and PLQY.[40]

To gain insight into the presence of the BPY ligand on the surface of the nanocrystals, the FTIR technique was employed. Fig. S6 (ESI†) displays the FTIR spectrum of both BPY and BPY-$CsPbBr_3$ PNCs. The peaks at 2855 and 2926 cm^{-1} are the characteristic peaks of C–H stretching vibrations of ($-CH_2$) and ($-CH_3$) groups of OAm, respectively. The peak at 2975 cm^{-1} is attributed to the stretching vibration of the aromatic C–H bond. The peak at 1640 cm^{-1} is due to the C=C functional group. The peak at 1384 cm^{-1} is due to the COO^- functional group.[41] The peak at 1564 cm^{-1} corresponds to the C–N stretching vibration. The characteristic peaks at 720–910 cm^{-1} are due to aromatic bending vibrations.[42] The prominent peak at 1468 cm^{-1} in the BPY ligand spectrum is due to the OH stretching vibration of the carboxylic acid, but the intensity of this peak decreased in BPY-$CsPbBr_3$ PNCs.[43] These results indicate that the BPY ligand binds with the Pb atom through oxygen atoms of the carboxylic group which effectively passivates the surface of the BPY-$CsPbBr_3$ PNCs. To further confirm the presence of BPY ligand on the surface of BPY-$CsPbBr_3$ PNCs, X-ray photoelectron spectroscopy (XPS) analysis was performed. The full spectrum scan exhibits the representative peaks of all the constituent elements Cs, Pb, Br, C, and O, as shown in Fig. S7 (ESI†). The two peaks at 724.13, and 738.07 eV correspond to the Cs $3d_{5/2}$ and Cs $3d_{3/2}$ orbitals (Fig. 3(a)), respectively, and show no shift in the peak position, which is consistent with previous reports.[44]

In the Pb 4f orbital (Fig. 3(b)), we observed a shift of 0.36 eV towards higher binding energy, which is relatively due to the strong interaction of the carboxyl group of BPY with the Pb^{2+} atom.[45] Furthermore, a slight shift of 0.13 eV in the Br 3d orbitals (Fig. 3(c)) confirms the strong interaction of the BPY ligand.[42] Thus, these results indicate an improvement in the interaction in the presence of the BPY ligand.

Table 1 Lifetime decay of pristine $CsPbBr_3$ PNCs and BPY-$CsPbBr_3$ PNCs

Sample	A_1 (%)	τ_1 (ns)	A_2 (%)	τ_2 (ns)	A_3 (%)	τ_3 (ns)	τ_{avg} (ns)	PLQY (%)	K_r (ns^{-1})	K_{nr} (ns^{-1})
Pristine $CsPbBr_3$ PNCs	56.80	2.22	36.09	10.00	7.11	41.59	20.67	64	0.030	0.016
BPY-$CsPbBr_3$ PNCs	32.45	3.44	55.47	13.94	12.08	46.57	25.80	88	0.034	0.004

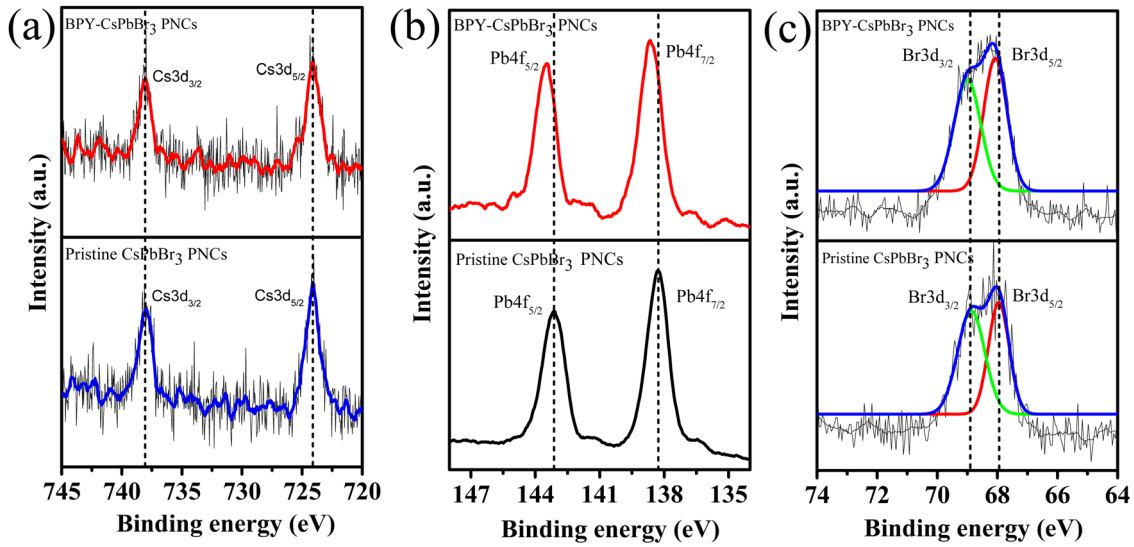

Fig. 3 XPS spectra for the narrow scan of (a) Cs, (b) Pb, and (c) Br.

The stability of PNCs is an integral part of device fabrication. In this context, we performed stability experiments for BPY-$CsPbBr_3$ PNCs. To determine the comparative thermal stability of pristine and BPY-$CsPbBr_3$ PNCs, a thermogravimetric analysis (TGA) was carried out. TGA spectra of pristine and BPY-$CsPbBr_3$ PNCs are depicted in Fig. 4(a). The spectra demonstrate that the majority of the weight of nanocrystals is lost in three distinct stages. Evaporation of the water that is present on the surface of the nanocrystals is responsible for the first-minute weight loss that occurs close to 100 °C. The second decomposition step starts from 180 °C and extends up to 450 °C. The release of surface-bound ligands BPY (boiling point >300 °C), OAm (boiling point ~350 °C), and OA (boiling point ~360 °C) is the cause of this weight loss. The third and most substantial weight loss indicates that BPY-$CsPbBr_3$ PNCs are stable up to 550 °C. After that temperature, the material loses its functional stability. TGA analysis shows that both the PNCs have almost comparative thermal stability. Furthermore, to find out more about the stability of BPY-$CsPbBr_3$ PNCs in ambient conditions, we stored the nanocrystals in the laboratory and performed PL and XRD studies with time. Fig. 4(b) displays the time-dependent PL spectra, which reveal that the BPY-$CsPbBr_3$ PNCs are still fluorescent after two months. Fig. 4(c) depicts a time-dependent XRD analysis, indicating that there are no observable alterations in the XRD pattern over time. We further investigated the stability of the BPY-$CsPbBr_3$ PNCs under hydrothermal conditions by adding 0.1 mL of water to 3 mL colloidal solution of BPY-$CsPbBr_3$

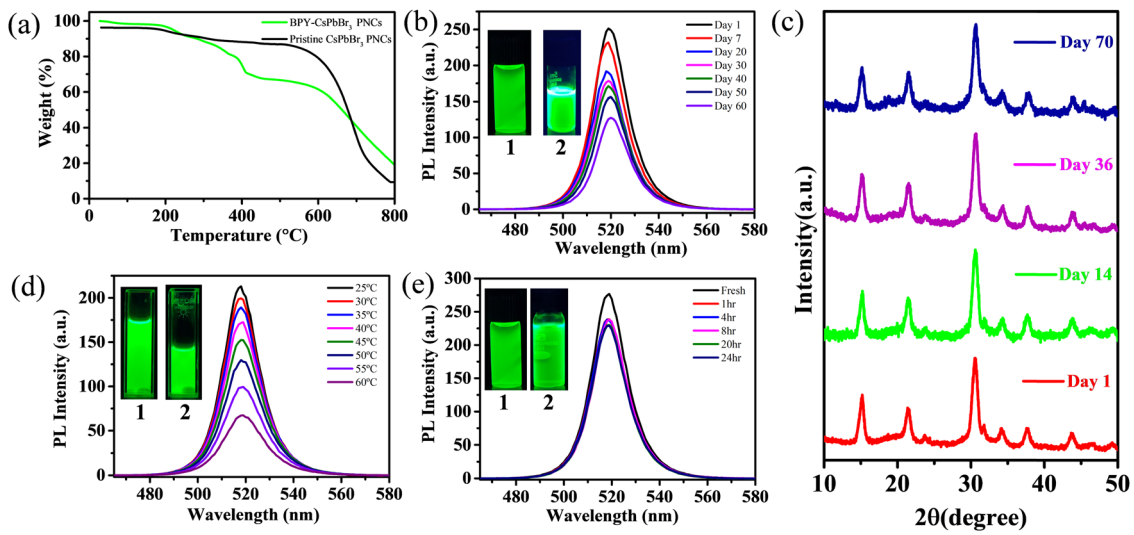

Fig. 4 (a) TGA of pristine and BPY-$CsPbBr_3$ PNCs; (b) time-dependent PL (inset shows the optical image 1 at day 1 and 2 at day 60); (c) time-dependent XRD pattern of BPY-$CsPbBr_3$ PNCs; (d) hydrothermal stability (inset shows the optical image 1 at room temperature and 2 at 60 °C); (e) photostability (inset shows the optical image 1 of fresh PNCs and 2 after 24 h of under UV light).

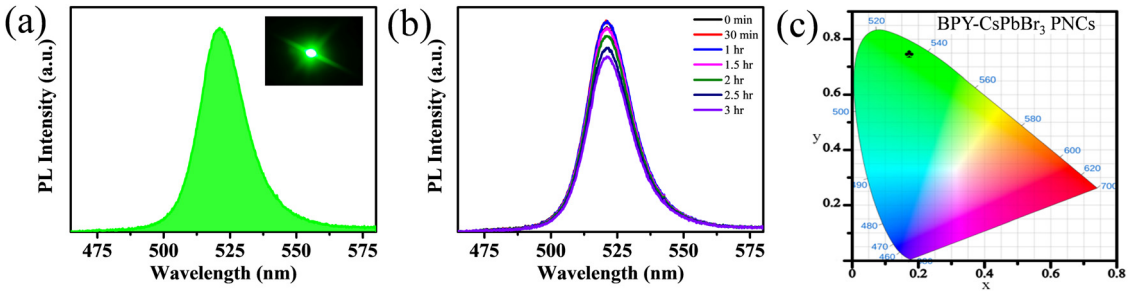

Fig. 5 (a) PL spectra of a down-converted LED (inset shows the photograph), (b) PL spectra from 0 h to 3 h, and (c) CIE chromaticity coordinates of the down-converted LED.

PNCs and recorded the PL spectra at elevated temperatures up to 60 °C. The BPY-$CsPbBr_3$ PNCs maintained their PL after heating up to 60 °C (Fig. 4(d)). For photostability, BPY-$CsPbBr_3$ PNC colloidal solution is kept under continuous UV irradiation (λ_{ex} = 365 nm) for 24 h. We found that PL is preserved even after 24 h of continuous UV irradiation (Fig. 4(e)). The results validate that the BPY-$CsPbBr_3$ PNCs under investigation have exhibited stability in normal environmental conditions for a duration exceeding two months as well as in different harsh conditions. Furthermore, we have listed the different bidentate ligands used along with their variable properties in Table S1 (ESI†) to demonstrate a comparison of our work with the previously reported literature.

To further investigate the potential of green emissive BPY-$CsPbBr_3$ PNCs for optoelectronic applications. We fabricate a down-converted green LED by coating BPY-$CsPbBr_3$ PNCs on a commercially available blue LED (λ_{ex} = 395 nm). The down-converted LED device shows a strong PL emission centered at 521 nm with a narrow full width at half maxima (fwhm) of 19 nm (Fig. 5(a)). In the inset of Fig. 5(a), the photograph of the green LED was taken inside a dark room. Fig. S8 (ESI†) shows the photograph of the LED under daylight. The time-dependent PL spectra of BPY-$CsPbBr_3$ PNCs were recorded under continuous working conditions from initial 0 h to 3 h, as shown in Fig. 5(b). The nanocrystals retain 86% of their initial PL after 3 h. The Commission Internationale de l'Eclairage (CIE) color coordinates of the LED are (0.17, 0.74) and the CIE chromaticity plot is given in Fig. 5(c). These results demonstrate that the synthesized nanocrystals have color stability after working for 3 h with no shift in the wavelength and are promising for optoelectronic applications.

Conclusion

In conclusion, bidentate BPY and OAm were used as capping ligands for the synthesis of highly green-emitting BPY-$CsPbBr_3$ PNCs. We studied the effect of BPY on the optical properties of BPY-$CsPbBr_3$ PNCs and found that BPY significantly boosts the optical properties. The BPY ligand effectively reduced the surface defects by strong interaction of the carboxyl group with lead atoms, which eventually enhanced the optical properties which is evidenced by performing PL, PLQY, and TCSPC characterization techniques. FTIR and XPS studies confirmed the presence of BPY on the BPY-$CsPbBr_3$ PNC surface. Meanwhile, XRD, SEM, and TEM studies reveal that there are no structural or morphological changes observed in the BPY-$CsPbBr_3$ PNCs compared to the pristine $CsPbBr_3$ PNCs. The stability-related studies prove that BPY-$CsPbBr_3$ PNCs are stable in the ambient environment for more than two months. Finally, a green down-converted LED was fabricated by drop-casting BPY-$CsPbBr_3$ PNCs on a blue LED. These results demonstrate the potential of BPY-$CsPbBr_3$ PNCs in light-emitting applications.

Conflicts of interest

There is no conflict of interest to declare for this work.

Acknowledgements

P. K. acknowledges Science and Engineering Research Board (CRG/2020/000702), New Delhi, India. A. K. and S. K. acknowledge CSIR, India, and S. G. and A. S. acknowledge MoE for their doctoral fellowship. M. B. acknowledges the Science and Engineering Research Board, India (CRG/2021/001744). The authors acknowledge Institute Instrumental Centre (IIC), and IIT Roorkee for instrumental facilities.

References

1 D. Zhang, S. W. Eaton, Y. Yu, L. Dou and P. Yang, *J. Am. Chem. Soc.*, 2015, **137**, 9230–9233.
2 X. Li, F. Cao, D. Yu, J. Chen, Z. Sun, Y. Shen, Y. Zhu, L. Wang, Y. Wei, Y. Wu and H. Zeng, *Small*, 2017, **13**, 1603996.
3 F. Liu, Y. Zhang, C. Ding, S. Kobayashi, T. Izuishi, N. Nakazawa, T. Toyoda, T. Ohta, S. Hayase, T. Minemoto, K. Yoshino, S. Dai and Q. Shen, *ACS Nano*, 2017, **11**, 10373–10383.
4 A. Jha, H. Shankar and P. Kar, *New J. Chem.*, 2022, **46**, 844–850.
5 A. Swarnkar, R. Chulliyil, V. K. Ravi, M. Irfanullah, A. Chowdhury and A. Nag, *Angew. Chem., Int. Ed.*, 2015, **127**, 15644–15648.

6 J. A. Sichert, Y. Tong, N. Mutz, M. Vollmer, S. Fischer, K. Z. Milowska, R. García Cortadella, B. Nickel, C. Cardenas-Daw, J. K. Stolarczyk, A. S. Urban and J. Feldmann, *Nano Lett.*, 2015, **15**, 6521–6527.
7 C. Wehrenfennig, G. E. Eperon, M. B. Johnston, H. J. Snaith and L. M. Herz, *Adv. Mater.*, 2014, **26**, 1584–1589.
8 M. V. Kovalenko, L. Protesescu and M. I. Bodnarchuk, *Science*, 2017, **358**, 745–750.
9 J. Song, J. Li, X. Li, L. Xu, Y. Dong and H. Zeng, *Adv. Mater.*, 2015, **27**, 7162–7167.
10 N. Ahn, D. Y. Son, I. H. Jang, S. M. Kang, M. Choi and N. G. Park, *J. Am. Chem. Soc.*, 2015, **137**, 8696–8699.
11 L. Dou, Y. M. Yang, J. You, Z. Hong, W. H. Chang, G. Li and Y. Yang, *Nat. Commun.*, 2014, **5**, 5404.
12 Y. Fu, H. Zhu, C. C. Stoumpos, Q. Ding, J. Wang, M. G. Kanatzidis, X. Zhu and S. Jin, *ACS Nano*, 2016, **10**, 7963–7972.
13 L. Protesescu, S. Yakunin, M. I. Bodnarchuk, F. Krieg, R. Caputo, C. H. Hendon, R. X. Yang, A. Walsh and M. V. Kovalenko, *Nano Lett.*, 2015, **15**, 3692–3696.
14 A. H. Slavney, R. W. Smaha, I. C. Smith, A. Jaffe, D. Umeyama and H. I. Karunadasa, *Inorg. Chem.*, 2017, **56**, 46–55.
15 Q. Zhong, M. Cao, H. Hu, D. Yang, M. Chen, P. Li, L. Wu and Q. Zhang, *ACS Nano*, 2018, **12**, 8579–8587.
16 H. Li, C. Jia, H. Li and X. Meng, *Chem. Commun.*, 2018, **54**, 6300–6303.
17 F. Krieg, S. T. Ochsenbein, S. Yakunin, S. Ten Brinck, P. Aellen, A. Süess, B. Clerc, D. Guggisberg, O. Nazarenko, Y. Shynkarenko, S. Kumar, C. J. Shih, I. Infante and M. V. Kovalenko, *ACS Energy Lett.*, 2018, **3**, 641–646.
18 H. Shankar, W. W. Yu, Y. Kang and P. Kar, *Sci. Rep.*, 2022, **12**, 7848.
19 P. Kour and S. P. Mukherjee, *J. Mater. Chem. A*, 2021, **9**, 6819–6826.
20 L. Yang, B. Fu, X. Li, H. Chen and L. Li, *J. Mater. Chem. C*, 2021, **9**, 1983–1991.
21 M. Qin, H. Xue, H. Zhang, H. Hu, K. Liu, Y. Li, Z. Qin, J. Ma, H. Zhu, K. Yan, G. Fang, G. Li, U. S. Jeng, G. Brocks, S. Tao and X. Lu, *Adv. Mater.*, 2020, **32**, 2004630.
22 J. de Roo, M. Ibáñez, P. Geiregat, G. Nedelcu, W. Walravens, J. Maes, J. C. Martins, I. van Driessche, M. V. Kovalenko and Z. Hens, *ACS Nano*, 2016, **10**, 2071–2081.
23 J. Pan, S. P. Sarmah, B. Murali, I. Dursun, W. Peng, M. R. Parida, J. Liu, L. Sinatra, N. Alyami, C. Zhao, E. Alarousu, T. K. Ng, B. S. Ooi, O. M. Bakr and O. F. Mohammed, *J. Phys. Chem. Lett.*, 2015, **6**, 5027–5033.
24 L. Protesescu, S. Yakunin, M. I. Bodnarchuk, F. Krieg, R. Caputo, C. H. Hendon, R. X. Yang, A. Walsh and M. V. Kovalenko, *Nano Lett.*, 2015, **15**, 3692–3696.
25 K. Vighnesh, S. Wang, H. Liu and A. L. Rogach, *ACS Nano*, 2022, **16**, 19618–19625.
26 J. Pan, Y. Shang, J. Yin, M. de Bastiani, W. Peng, I. Dursun, L. Sinatra, A. M. El-Zohry, M. N. Hedhili, A. H. Emwas, O. F. Mohammed, Z. Ning and O. M. Bakr, *J. Am. Chem. Soc.*, 2018, **140**, 562–565.
27 J. Qiu, W. Xue, W. Wang and Y. Li, *Dyes Pigm.*, 2022, **198**, 109806.
28 J. Y. Woo, Y. Kim, J. Bae, T. G. Kim, J. W. Kim, D. C. Lee and S. Jeong, *Chem. Mater.*, 2017, **29**, 7088–7092.
29 S. Ghosh and P. Kar, *Inorg. Chem.*, 2022, **61**, 10079–10088.
30 B. A. Koscher, J. K. Swabeck, N. D. Bronstein and A. P. Alivisatos, *J. Am. Chem. Soc.*, 2017, **139**, 6566–6569.
31 F. Liu, Y. Zhang, C. Ding, S. Kobayashi, T. Izuishi, N. Nakazawa, T. Toyoda, T. Ohta, S. Hayase, T. Minemoto, K. Yoshino, S. Dai and Q. Shen, *ACS Nano*, 2017, **11**, 10373–10383.
32 Y. Yue, S. Liu, B. Qi, Z. Su, G. Li, C. Wang and D. Zhu, *ACS Appl. Mater. Interfaces*, 2021, **13**, 21645–21652.
33 A. Dutta, R. K. Behera, P. Pal, S. Baitalik and N. Pradhan, *Angew. Chem., Int. Ed.*, 2019, **131**, 5608–5612.
34 Y. Li, M. Cai, M. Shen, Y. Cai and R. J. Xie, *J. Mater. Chem. C*, 2022, **10**, 8356–8363.
35 D. Chen, P. K. Ko, C. H. A. Li, B. Zou, P. Geng, L. Guo and J. E. Halpert, *ACS Energy Lett.*, 2023, **8**, 410–416.
36 M. Liu, Q. Wan, H. Wang, F. Carulli, X. Sun, W. Zheng, L. Kong, Q. Zhang, C. Zhang, Q. Zhang, S. Brovelli and L. Li, *Nat. Photonics*, 2021, **15**, 379–385.
37 J. Stachurski, S. Tamariz, G. Callsen, R. Butté and N. Grandjean, *Light: Sci. Appl.*, 2022, **11**, 114.
38 Y. Xing, L. Wang, D. Yang, Z. Wang, Z. Hao, C. Sun, B. Xiong, Y. Luo, Y. Han, J. Wang and H. Li, *Sci. Rep.*, 2017, **7**, 45082.
39 J. Y. Woo, Y. Kim, J. Bae, T. G. Kim, J. W. Kim, D. C. Lee and S. Jeong, *Chem. Mater.*, 2017, **29**, 7088–7092.
40 X. Zhu, Z. Pan, T. Xu, X. Shao, Z. Gao, Q. Xie, Y. Ying, W. Pei, H. Lin, J. Wang, X. Tang, W. Chen and Y. Liu, *Inorg. Chem.*, 2023, **62**, 9190–9198.
41 D. Patra and S. P. Singh, *J. Phys. Chem. C*, 2023, **127**, 9397–9406.
42 V. G. V. Dutt, S. Akhil, R. Singh, M. Palabathuni and N. Mishra, *J. Phys. Chem. C*, 2022, **126**, 9502–9508.
43 P. S. Calefi, A. O. Ribeiro, A. M. Pires and O. A. Serra, *J. Alloys Compd.*, 2002, **344**, 285–288.
44 K. A. Huynh, S. R. Bae, T. Van Nguyen, H. H. Do, D. Y. Heo, J. Park, T. W. Lee, Q. Van Le, S. H. Ahn and S. Y. Kim, *ACS Photonics*, 2021, **8**, 1979–1987.
45 V. G. V. Dutt, S. Akhil, R. Singh, M. Palabathuni and N. Mishra, *ACS Appl. Nano Mater.*, 2022, **5**, 5972–5982.